Caram, H. S., and N. R. Amundson, "Diffusion and Reaction in a Stagnant Boundary Layer About a Carbon Particle," *Ind. Eng. Chem. Fundamentals*, **16**, 171 (1977).
Chen, T. P., and S. C. Saxena, "A Mechanistic Model Applicable to Coal Combustion in Fluidized Beds," *AIChE Symposium Ser. No. 176*, **74**, 149 (1978).
Davidson, J. F., and D. Harrison, *Fluidized Particles*, Cambridge Univ. Press (1963).
Exxon Research and Engineering Company, "Studies of the Pressurized Fluidized Bed Coal Combustion Process," EPA—600/7-76-011, Linden, N.J. (1976).
Field, M. A., D. W. Gill, B. B. Morgan and P. G. W. Hawksley, "Combustion of Pulverized Coal," BCURA (1967).
Fine, D. H., S. M. Slater, A. F. Sarofim and G. C. Williams, "Nitrogen in Coal as a Source of Nitrogen Oxide Emission from Furnaces," *Fuel*, **53**, 120 (1974).
Fournol, A. B., M. A. Bergougnou and C. G. J. Baker, "Dilute Phase Hold-Up in a Large Gas Fluidized Bed," *Can. J. Chem. Eng.*, **51**, 401 (1973).
Gibbs, B. M., F. J. Pereira and J. M. Beer, "Coal Combustion and NO Formation in an Experimental Fluidized Bed," *Inst. Fuel Symp. Series*, Paper D6 (1975).
Gibbs, B. M., "A Mechanistic Model for Predicting the Performance of a Fluidized Bed Coal Combustor," *ibid.*, Paper A5 (1975).
Gordon, A. L., and N. R. Amundson, "Modeling of Fluidized Bed Reactors—IV: Combustion of Carbon Particles," *Chem. Eng. Sci.*, **31**, 1163 (1976).
Gregory, D. R., and R. F. Littlejohn, "A Survey of Numerical Data on the Thermal Decomposition of Coal," *The BCURA Monthly Bulletin*, **29**, No. 6, 173 (1965).
Horio, M., S. Mori and I. Muchi, "A Model Study for the Development of Low $No_x$ Fluidized Bed Combustors," Proc. of 5th FBC Conference, Washington, D.C. (1977).
Horio, M., and C. Y. Wen, "Analysis of Fluidized Bed Combustion of Coal With Limestone Injection," Proc. of Int. Fluidization Conference, Pacific Grove, Calif. (1975).
———, "Simulation of Fluidized Bed Combustors: Part I Combustion Efficiency and Temperature Profile," *AIChE Symposium Ser. No. 176*, **74**, 101 (1978).
Hottel, H. C., G. C. Williams, N. M. Nerheim and G. R. Schneider, "Burning Rate of Carbon Monoxide," 10th International Symposium on Combustion, 111 (1965).
Ishida, M., and C. Y. Wen, "Effect of Solid Mixing on Non-Catalytic Solid-Gas Reactions in a Fluidized Bed," *AIChE Symposium Ser., No. 128*, **69**, 1 (1973).
Loison, R., and R. Chuvwin, "Pyrolyse Rapide du Charbon," *Chemie et. Industrie*, **91**, 269 (1964).
Merrick, D., and J. Highley, "Particle Size Reduction and Elutriation in a Fluidized Bed Process," *AIChE Symposium Ser. No. 137*, **70**, 366 (1974).
Mori, S., and C. Y. Wen, "Estimation of Bubble Diameter in Gaseous Fluidized Beds," *AIChE J.*, **21**, 109 (1975).
NASA Lewis Research Center, Cleveland, Ohio, Private Communication (1978).
National Coal Board, "Reduction of Atmospheric Pollution," EPA-PB-210-673, London, England (1971).
Nazemi, A., M. A. Bergougnou and C. G. J. Baker, "Dilute Phase Hold-Up in a Large Gas Fluidized Bed," *AIChE Symposium Ser. No. 141*, **70**, 98 (1974).
Oguma, A., N. Yamada, T. Furusawa and D. Kunii, "Reduction Reaction Rate of Char With NO," Preprint for 11th Fall Meeting of Soc. of Chem. Eng., Japan, 121 (1971).
Park, D., O. Levenspiel and T. J. Fitzgerald, "A Model for Large Scale Atmospheric Fluidized Bed Combustors," paper presented at 72nd Annual AIChE Meeting, San Francisco, Calif. (Nov., 1979).
Pereira, F. J., and J. M. Beer, "A Mathematical Model of NO Formation and Destruction in Fluidized Combustion of Coal," *Fluidization*, Proc. of Second Eng. Foundation Conf., Trinity College, Cambridge, England (1978).
Rajan, R., R. Krishnan and C. Y. Wen, "Simulation of Fluidized Bed Combustion: Part II: Coal Devolatilization and Sulphur Oxides Retention," *AIChE Symposium Ser. No. 176*, **74**, 112 (1978).
Sarofim, A. F., and J. M. Beer, "Modeling of Fluidized Bed Combustion," *Colloquium on Coal Combustion*, 189 (1979).
Wen, C. Y., and L. H. Chen, "A Model for Coal Pyrolysis," Division of Fuel Chemistry, ACS Preprint, **24**, 141 (1979).
Wen C. Y., and L. T. Fan, *Model for Flow Systems and Chemical Reactors*, Dekker, New York (1975).
Wen, C. Y., and M. Ishida, "Reaction Rate of Sulphur Dioxide With Particles Containing Calcium Oxide," *Environ. Sci. Tech.*, **1**, 103 (1973).
Wen, C. Y., and Y. H. Yu, "A Generalized Method for Predicting the Minimum Fluidization Velocity," *AIChE J.*, **12**, 610 (1966).
Yates, J. G., and P. N. Rowe, "A Model for Chemical Reaction in the Freeboard Region Above a Fluidized Bed," *Trans. Inst. Chem. Engrs.*, **55**, 137 (1977).
Zenz, F. A., and N. A. Weil, "A Theoretical-Empirical Approach to the Mechanism of Particle Entrainment from Fluidized Beds," *AIChE J.*, **4**, 472 (1958).

*Manuscript received May 14, 1979; revision received January 17, and accepted January 23, 1980.*

# Nucleation and Evolution of Slag Droplets in Coal Combustion

**KWAN H. IM**

**and**

**PAUL M. CHUNG**

**Argonne National Laboratory**
**Argonne, Illinois**

**Kinetics governing the nucleation and size variation of the slag droplets are first analyzed. Governing conservation equations are then formulated for the droplets and the surrounding gas-vapor mixture. These equations are solved numerically for the environments representing a typical flow through the channel and diffuser of a coal fired, MHD, power generation system. The average droplet size, total number density and the droplet size distribution are found to be rather strongly influenced by the total slag mass fraction and the supersaturation ratio.**

## SCOPE

One of the added complexities associated with the flow of the coal generated plasma, through the MHD channel and the after gas system, is caused by the residual slag invariably carried over to the MHD channel from the coal combustor (see, for instance, Heywood and Womack, 1969; Way, 1974; Chung and Smith, 1977; Ubhayaker et al., 1976). The slag may be both in a liquid and vapor phase. In addition to physically interacting with the electrode surfaces, the slag droplets, either carried into the channel or formed through nucleation, act as a strong electron sink (Martinez-Sanchez et al., 1977). Thus, the slag in the plasma could substantially affect the generator performance. Also, radiative heat transfer from the combustion gas to the surroundings is strongly influenced by the number density and size distribution of the droplets. In the subsequent after gas treatment system, condensation and removal of the slag must be accomplished among other gas cleaning and energy recovery processes. It is clear, therefore, that

, Paul M. Chung is at the University of Illinois, Chicago Circle, Illinois.

0001-1541-80-3707-0655-$01.05. 

understanding of the nucleation and subsequent behavior of the various size droplets is necessary in order to design an optimal coal fired MHD system.

A study is made in this paper of the formation of the slag droplets from vapor and the evolution of the droplet sizes taking place in the generator or after gas system. Specifically, it is considered that a gaseous mixture containing certain initial amounts of slag vapor and slag droplets is given. Also given initially are the size distribution of the slag droplets and properties of the gas mixture. The gas property is then considered to vary in an arbitrary manner with respect to time. The present analysis describes the nucleation and time variation of the droplet size distribution. The analysis is based on the solution of the spray equation (see Williams, 1965) in the time-size coordinate system with appropriate kinetics describing the nucleation and the droplet size variation.

A related analysis has been made by Martinez-Sanchez et al. (1977). In the present work, many of the previous approximations have been relaxed. The size distribution was not considered in the previous work. Further discussion of the Martinez-Sanchez solution will be given in a separate section.

The text begins with construction of the governing conservation equation for the droplets. The kinetic descriptions of the droplet growth and nucleation necessary for the droplet equation are also developed. The governing equation for the gas phase mixture is then formulated. The coupled set of the governing equations of droplets and gas mixtures is then solved, and typical results of the solution are discussed.

## CONCLUSIONS AND SIGNIFICANCE

Nucleation and the droplet growth were analyzed for the slag vapor and droplet ridden combustion gas stream. Numerical solutions were obtained for environments representing the flows through the channel and diffuser.

It was found that the partial differential equation governing the droplets is very unstable because of the precipitous manner in which the nucleation rate varies and the strong dependence of the droplet growth rate on the droplet size. This difficulty was circumvented by a logarithmic transformation of the independent variable $r$.

The numerical solutions showed that evolution of the droplet size distribution proceeds through a succession of rather delicate balances between the size dependent condensation and evaporation rates and the nucleation rate. These balances are largely dictated by the amount of ash carryover and the supersaturation ratio.

Evaporation and or growth at an early stage of the submicron size droplets and the subsequent nucleation of the extremely small droplets engender a bimodal size distribution either in the channel or in the diffuser, depending on the supersaturation ratio. This bimodal nature is preserved through the diffuser.

The higher slag content was found to trigger nucleation prematurely in the channel such that a relatively smaller portion of the vapor nucleates. The remaining portion of the vapor condenses on droplets and causes rapid growth of the droplets. The higher slag content, therefore, squeezes the entire size distribution toward the larger radius region of the spectrum. Also, it results in a reduced droplet number density and increased mean radius at the end of the diffuser.

## EQUATIONS FOR DROPLETS

We consider a spatially homogeneous mixture of gas and slag droplets at $t = 0$. All necessary properties of the mixture including the number density and size distribution of the droplets are considered to be given at the initial time. Then the time evolution of the number density of the various size droplets is governed by the spray equation (see Williams, 1965):

$$\frac{\partial n(r, t)}{\partial t} + \frac{\partial}{\partial r}[rn(r, t)] = J(r, t)\,\delta(r - r^*) \qquad (1)$$

In the above equation, $n(r, t)$ denotes the number density of the droplets with the radii between $r$ and $r + dr$ at time $t > 0$.

In order to render Equation (1) self-contained, the rates of droplet growth and nucleation must be known. Expressions for these quantities are derived in the following.

### Rate of Droplet Growth

Nucleation is expected to engender slag droplets whose diameters are of the order of 10 angstroms, as seen in Feder et al. (1966), Dunning (1969), and Anders (1969). On the other hand, the droplets carried out of the combustor are expected to have sizes of the order of several microns. Typical mean free path in the gas flowing in the MHD system is estimated to be of the order of 1 $\mu$. Therefore, the droplet gas interactions of present interest would encompass the free molecular to the mixed interaction regimes, that is, the regimes where the Knudsen number is very large down to the order of 0.1. The droplet growth rate is analyzed in the following to take account of the interaction regimes present yet in a sufficiently simplified manner so as to render the analysis tractable.

Consider the droplet of radius $r$ and the surrounding gas shown in Figure 1. After the conventional simplified method of analysis of the Knudsen flow regime (see Sedunov, 1974; Kogan, 1969), we divide the gas surrounding the droplet into two layers,

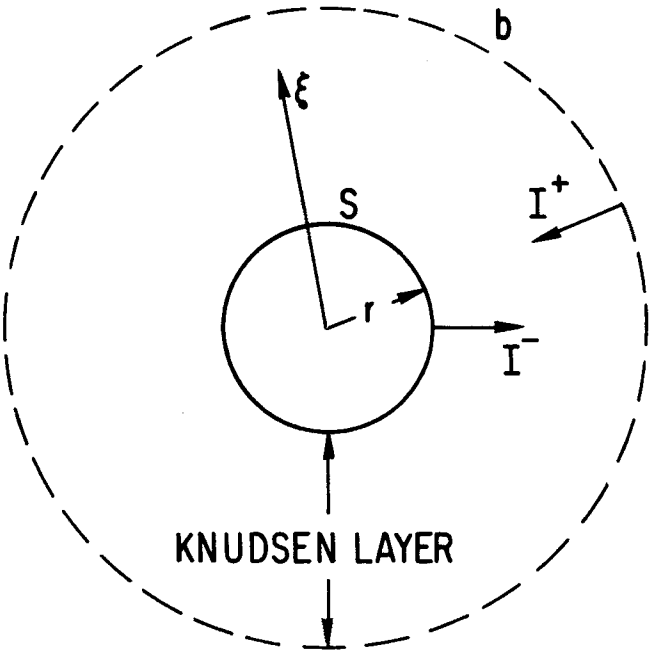


Figure 1. Particle growth evaporation model.

the layer adjacent to the droplet surface of one mean free path thickness (Knudsen layer) and that outside of this layer. The interface between the two layers is labeled as $b$ in Figure 1. It is assumed that state of the gas at $b$ and beyond is in kinetic equilibrium; that is, the velocity distribution is near Maxwellian owing to the numerous gas-gas collisions in the region of $(\zeta - r) > \lambda$. No gas-gas collision occurs between $b$ and the droplet surface $s$. It is also assumed that the slag vapor molecules emitted from the surface $s$ are in a kinetic equilibrium at $T_s$.

Rate of emission of the slag vapor molecules from the surface $s$ can be expressed as

$$I_- = 4\pi r^2 \left(\frac{n_{cs} v_{cs}}{4}\right) \exp[\phi/(kT_s)] \tag{2}$$

where $\phi$ is the energy function which represents the energy needed to form the droplet of a given radius. It will be expressed in terms of the surface tension and other pertinent properties later. Since it has been assumed that the gas at the boundary $b$ is in kinetic equilibrium, the mass rate of vapor leaving $b$ toward the droplet surface is

$$I_+ = r\pi r^2 (n_{cb} v_{cb}/4) \tag{3}$$

Growth rate of the droplet size is then given by

$$\dot{r} = m_c (I_+ - I_-)/(4\pi r^2 \rho_l) \tag{4}$$

Our purpose at hand is to make the above equation for $\dot{r}$ explicit by determining the variables defining $I_-$ and $I_+$. With this in mind, we proceed as follows.

We construct the vapor mass and total energy balances at the interface $b$ as

$$4\pi(r + \lambda) D_v (n_c - n_{cb}) = 4\pi r^2 \left[\frac{n_{cb} v_{cb}}{4} - \frac{n_{cs} v_{cs}}{4} \exp\left(\frac{\phi}{kT_s}\right)\right] \tag{5}$$

$$4\pi(r + \lambda) K (T_g - T_b) = 4\pi r^2 \left[\frac{n_{gb} v_{gb}}{4} \left(\frac{3}{2} kT_b\right) - \frac{n_{gs} v_{gs}}{4} \frac{3}{2} kT_s\right] \tag{6}$$

$T_g$ and $n_c$ without the subscript $b$ or $s$ denote the properties in the free gas stream. The slag vapor constitutes only a trace in the gas mixture. Therefore, its effect on the above energy equation is neglected.

Since the only properties given are those in the free stream, Equations (5) and (6) contain twelve unknowns: $n_{gs}$, $n_{cb}$, $n_{cs}$, $n_{gb}$, $v_{gb}$, $v_{cb}$, $T_b$, $v_{cs}$, $D_v$, $v_{gs}$, $K$ and $T_s$. Seven simple relationships, however, can be readily obtained from the kinetic theory as

$$v_{gb} = \left(\frac{8kT_b}{\pi m_g}\right)^{\frac{1}{2}}, \qquad v_{gs} = \left(\frac{8kT_s}{\pi m}\right)^{\frac{1}{2}}$$

$$v_{cb} = \left(\frac{8kT_b}{\pi m_c}\right)^{\frac{1}{2}}, \qquad v_{cs} = \left(\frac{8kT_s}{\pi m_c}\right)^{\frac{1}{2}}$$

$$n_{gs} v_{gs} = n_{gb} v_{gb}, \tag{7}$$

$$D_v = \frac{3}{5} r \left(\frac{8kT_g}{\pi m_c}\right)^{\frac{1}{2}} Kn,$$

$$K = \frac{15}{8} k\, n_{ig} \left(\frac{8kT_g}{\pi m}\right)^{\frac{1}{2}} r\, Kn$$

In addition, $n_{cs}$ is the number density of the vapor molecules corresponding to the saturated state at $T_s$. Therefore, the relationship

$$n_{cs} = n_{cs}(T_s) \tag{8}$$

can be considered known. Also, for simplicity, we assume that

$$n_{gb} = n_g \tag{9}$$

where $n_g$ is the noncondensible gas molecular number density in the free stream. One additional relationship would comprise the necessary twelve equations for the twelve unknowns. This equation is obtained by constructing a complete energy balance on the droplet as

$$4\pi r^2 \left\{\left[\frac{n_{gb} v_{gb}}{4} \left(\frac{3}{2} kT_b\right) - \frac{n_{gs} v_{gs}}{4} \left(\frac{3}{2} kT_s\right)\right] + \left[\frac{n_{cb} v_{cb}}{4} - \frac{n_{cs} v_{cs}}{4} \exp\left(\frac{\phi}{kT_s}\right)\right] m_c L\right\} = 0 \tag{10}$$

For the small size droplets of the present interest, the radiation heat transfer is neglected in comparison with the convective heat transfer. The quantity in the first square bracket represents the sensible heat transfer to the droplet by molecular conduction, and that in the second square bracket represents the latent heat transfer to the droplet by condensation. A quasi steady state condition was used in constructing Equation (10). A quasi steady state prevails, since the free stream conditions change at a sufficiently slow rate as compared to the rates at which the continuum and Knudsen layers surrounding the droplet and the droplet itself can respond to the change.

Equations (5) through (10) constitute twelve algebraic equations with the same number of unknowns. These equations are solved, and the following equations are obtained for the droplet growth rate $\dot{r}$ given by Equation (4):

$$\dot{r} = \frac{12}{5} \frac{Kn\, P_{\text{sat}}(T_g)}{\rho_l \sqrt{2\pi R_v T_g}} f \left[S - \left(\frac{T_g}{T_s}\right)^{\frac{1}{2}} \frac{\text{sat}(T_s)}{P_{\text{sat}}(T_g)} \exp\left(\frac{\phi}{kT_s}\right)\right] \tag{11}$$

where

$$T_s = T_g \left[1 + \frac{f P_{\text{sat}} L\, [(S - \exp(\phi/kT_g)]}{\frac{25}{8} PT_g g \sqrt{R_t R_g} + P_{\text{sat}} L f \exp(\phi/kT_g) \left(\frac{L}{R_t T_g} - \frac{\phi}{kT_g} - \frac{1}{2}\right)}\right] \tag{12}$$

The two functions of the Knudsen number, $f$ and $g$, are defined as

$$f = \frac{1 + Kn}{1 + \frac{15}{2} Kn\,(1 + Kn)} \tag{13}$$

$$g = \frac{1 + Kn}{1 + 15 \left(\frac{\gamma - 1}{\gamma + 1}\right) Kn(1 + Kn)}$$

The supersaturation ratio $S$ is defined as

$$S = P_v(T_g)/P_{\text{sat}}(T_g) \tag{14}$$

In deriving Equation (11), the molecular number densities are replaced by appropriate partial pressures via equation of state of ideal gas.

Construction of the droplet growth rate equation, Equation (11), is complete as soon as we define the energy function $\phi$. The work required to construct a spherical droplet from the same volume out of a bulk of the liquid is defined as the energy function $\phi$. It can be expressed (see Dunning, 1969; Anders, 1969) in terms of the surface tension $\sigma$ as

$$\phi = \frac{2\sigma m_c}{\rho_l r} \tag{15}$$

### Homogeneous Nucleation

Collisions and the attendant cohesions of the monomers are considered to cause nucleation. Zeldovich, upon this consideration, formulated the following equation for the nucleation rate (see Feder et al., 1966; Dunning, 1969; Anders, 1969; Reiss and Katz, 1967; Reiss et al., 1968; Katz and Ostemier, 1967; Wegner et al., 1972):

$$J = \beta(4\pi r^2)\, ZC_1 \exp[-\Delta G_n^*/(kT_g)] \tag{16}$$

$C_1$ is the concentration of the monomer, and $G_n^*$ is the Gibbs free energy function for the formation of $n$-mers with the radius $r^*$. The critical radius $r^*$ of the $n$-mers or the droplets, first formed through nucleation, is given by the Gibbs-Thompson relationship found in Feder et al. (1966), Dunning (1969) and Anders (1969) as

$$r^* = \frac{2\sigma\hat{v}}{kT_g \ln S} \tag{17}$$

Through manipulation of Equations (16) and (17), and with certain other classical thermodynamic relationships, the following equation is derived in Feder et al. (1966), Dunning (1969) and Anders (1969):.

$$J = \left(\frac{2}{\pi}\right)^{\frac{1}{2}} \left(\frac{P_v}{kT_g}\right)^2 \hat{v}\left(\frac{\sigma}{m_c}\right)^{\frac{1}{2}} \exp\left(\frac{-4\pi}{3} r^{*2}\sigma/kT_g\right) \tag{18}$$

Subsequent to derivation of the above classical expression, a few somewhat different expressions have been derived for $J$ (see, for instance, Wegner et al., 1972; Lothe and Pound, 1968). Because of the difficulties in determining the constants appearing in these subsequent theories, it is not clear whether these theories are actually improvements over the classical theory of Equation (18). In the present analysis, therefore, we shall employ Equation (18).

Before leaving the discussion of nucleation rate, we note that an assumption has been made in the derivation of Equation (18) that a statistical equilibrium exists among the $n$-mers. This assumption is questionable for the extremely low vapor concentrations where collisions among the $n$-mers are insufficient to maintain the equilibrium. However, in view of the rather large disagreement which exists between the various equilibrium results, an attempt at this stage to include the nonequilibrium aspect does not seem justifiable.

With the expressions for $\dot{r}$ and $J$ derived, Equations (11) and (18), the spray equation, Equation (1), is self-contained. In order to complete the governing set of equations, we must now describe the behavior of the gas streams.

## EQUATIONS FOR THE GAS PHASE

It is considered in the present problem that variations with respect to time of the bulk gas temperature and pressure are given.

On the other hand, conservation of the slag in the system must be enforced. For this purpose, we construct the following equation governing the slag vapor concentration:

$$\frac{\partial \rho_v}{\partial t} = -4\pi\rho_l \int_{r_0}^{\infty} r^2 \dot{r} n(r, t)\, dr - \frac{4\pi}{3}\rho_l (r^*)^3 J(r^*, t) + \frac{\rho_v}{\rho_g}\frac{\partial \rho_g}{\partial t} \tag{19}$$

Equation (19) for the slag vapor is, of course, coupled with the spray equation, Equation (1), governing the droplets.

## SOLUTION OF THE GOVERNING EQUATIONS

### Governing Equations

The spray equation, Equation (1), the vapor conservation equation, Equation (19), and the expressions for $\dot{r}$ and $J$ given by Equations (11), (12) and (18) are first reproduced here for completeness:

$$\frac{\partial n(r, t)}{\partial t} + \frac{\partial}{\partial r}[\dot{r}\, n(r, t)] = J(r, t)\, \delta(r - r^*) \tag{20}$$

$$\frac{\partial \rho_v}{\partial t} = -4\pi\rho_l \int_0^{\infty} r^2 \dot{r}\, n(r, t) dr - \frac{4\pi}{3}\rho_l (r^*)^3 J(r^*, t) + \frac{\rho_v}{\rho_g}\frac{\partial \rho_g}{\partial t} \tag{21}$$

$$\dot{r} = \frac{12}{5}\frac{Kn\, P_{\text{sat}}(T_g)}{\rho_l\sqrt{2\pi R_v T_g}} f\left[S - \left(\frac{T_g}{T_s}\right)^{1/2}\frac{P_{\text{sat}}(T_s)}{P_{\text{sat}}(T_g)} \exp\left(\frac{\phi}{kT_s}\right)\right] \tag{22}$$

$$T_s = T_g\left[1 + \frac{f P_{\text{sat}} L[S - \exp(\phi/kT_g)]}{\frac{25}{8} P T_g g\sqrt{R_v R_g} + P_{\text{sat}} L f \exp(\phi/kT_g)\left(\frac{L}{R_v T_g} - \frac{\phi}{kT_g} - \frac{1}{2}\right)}\right] \tag{23}$$

$$J(r^*, t) = \frac{2}{11}\left(\frac{P_v}{kT_s}\right)^2 \hat{v}\left(\frac{\sigma}{m_c}\right)^{\frac{1}{2}} \exp\left[-\frac{4\pi}{3} r^{*2}\sigma/(kT_g)\right] \tag{24}$$

where

$$f = \frac{1 + Kn}{1 + \frac{15}{2} Kn(1 + Kn)}$$

$$g = \frac{1 + Kn}{1 + 15\left(\frac{\gamma - 1}{\gamma + 1}\right) Kn(1 + Kn)}$$

$$s = P_v(T_g)/P_{\text{sat}}(T_g) \tag{25}$$

$$r^* = \frac{2\sigma\hat{v}}{kT_g \ln S}$$

### Initial and Boundary Conditions

The two differential equations, Equations (20) and (21), require two initial and one boundary conditions. The given initial droplet size distribution and slag pressure constitute the initial conditions. They are written as, at $t = 0$

$$n(r, t) = n(r, 0), \qquad P_v(T_g, t) = P_v(T_g, 0) \tag{26}$$

The boundary condition with respect to $r$ is, at $r = r_0$

$$n(r_0, t) = 0 \tag{27}$$

Solution of the equations is sought for $r > r_0$. The smallest droplet size $r_0$ is an arbitrary cutoff radius defined such that only the particles of radius larger than $r_0$ are considered to be droplets. In the present computation, we shall take $r_0 = 4$ angstroms. Provided that $r_0 \leq r^*$, solution of the problem is practically independent of $r_0$.

### Auxiliary Conditions

As mentioned previously, variations with respect to time of the pressure and temperature of the gas mixture $P(t)$ and $T_g(t)$ are given.

With Equation (25) substituted into Equation (20) to (24), these equations comprise five equations governing the five unknown functions, $n$, $\dot{r}$, $J$, $\rho_v$ and $T_s$. Their initial and boundary

conditions are given by Equations (26) and (27). We have now constructed a self-consistent boundary value problem.

### Method of Solution

Equation (21) is essentially a first-order differential equation with respect to $t$ only. With $\dot{r}$ and $J$ given by Equations (22) and (24), no real difficulty is expected in integrating this equation.

Equation (20), on the other hand, is a full partial differential equation with respect to $t$ and $r$. Direct application of a finite-difference scheme encountered a rather severe stability difficulty. The main cause of the difficulty lies in the fact that the nucleation and droplet growth rates are strongly $r$ and $t$ dependent. The nucleation, in fact, takes place at $r = r^*$ only. The droplet growth rate, as seen in Equation (22), rather precipitously increases as a certain value of $S$ is reached and as precipitously falls as the $S$ changes. Also, the growth rate is a strong function of the drop size $r$ through $kn$ and $\phi$. At a given time, $r$ may be positive for certain narrow region of the size spectrum and negative for another narrow region, simultaneously. After a certain amount of numerical experimentations, this difficulty was circumvented by the logarithmic transformation of $r$:

$$\zeta = \frac{1}{4}\left[\ln\left(\frac{r}{r_p}\right)\right]^{\frac{1}{4}} \tag{28}$$

With the stability problem solved, Equations (20) to (24) are solved numerically by employing the two-step Lax-Wendroff procedure found in Richtmyer and Morton (1967). Typical results obtained will be discussed subsequently following discussion of the Martinez-Sanchez model.

## COMPARISON WITH MARTINEZ-SANCHEZ ANALYSIS

The previous study of Martinez-Sanchez et al. (1977) is closely related to the present analysis. There are three basic differences between the present and the Martinez-Sanchez analysis.

1. In the earlier work of Martinez-Sanchez (1977), the first three moment equations of the spray equation, Equation (2), were analyzed instead of the spray equation itself. Hence, the analysis was carried out for the total number density $N_0$ and for the averaged quantities (moments) $\bar{r}$ and $\overline{r^2}$. No solution for the size distribution could be obtained in this method. In the present study, the spray equation is directly solved, and this enables one to study the evolution of the droplet size distribution as well as the various averaged quantities.

2. Interaction between the droplets and the surrounding gases is considered in the previous work to take place according to a free molecular description. This is not quite correct for a typical MHD system environment, where the Knudsen number could be as small as 0.1. In the present study, a more general description is employed which is valid for all interaction regimes between the free molecular and continuum limits.

3. Martinez-Sanchez et al. (1977) neglected the effect of the droplet surface tension on the heat and mass transfers between the droplets and the surrounding gases; that is, the energy function $\phi$ was set to zero. For the small droplets considered, the surface tension plays an important role in the droplet growth and vaporization, and this fact is taken into account in the present analysis.

## RESULTS AND DISCUSSION

The actual problem analyzed consists of the spatially homogeneous mixture whose properties are varying with respect to time. When applied to a steady flow problem, therefore, the present analysis constitutes a Lagrangian solution. Transformation to an Eulerian system can be accomplished for one-dimensional steady flow problem by the use of the relationship

$$t = \int \frac{dx}{u} \tag{29}$$

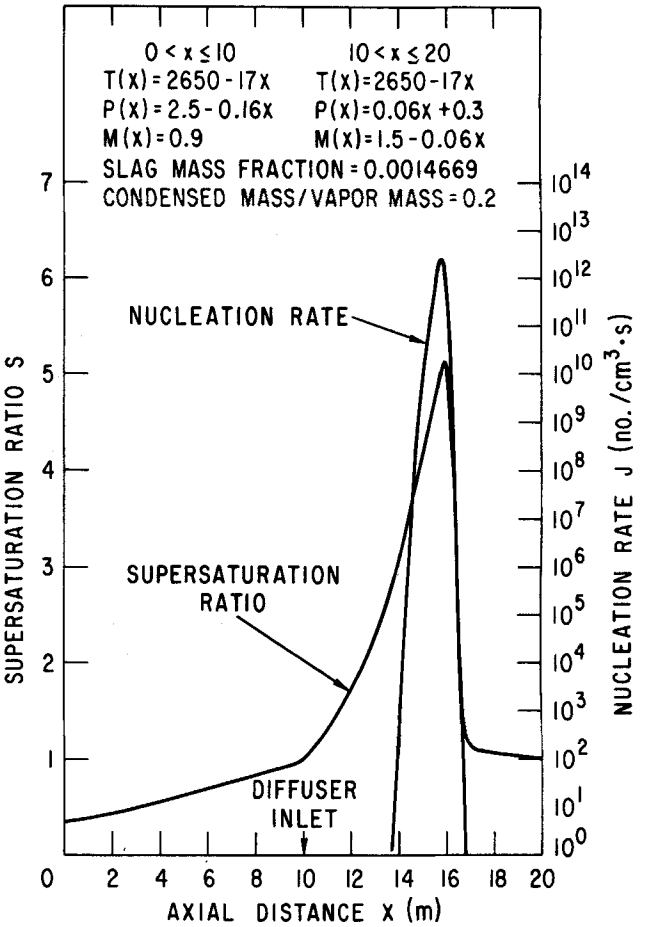


**Figure 2. Supersaturation ratio and nucleation rate through channel and diffuser for approximately 10% ash carryover.**

This relationship is employed in the following to describe the flow through a channel and diffuser combination by the use of the present solution.

The initial conditions to be specified were discussed in the sections following Equation (25).

Results of three different sets of computations are shown on Figures 2 to 10. The three sets are chosen from typical conditions found at the inlet to the MHD channel such that, among other things, effects of the supersaturation ratio and the amount of ash carryover on the final droplet size distribution can be elucidated. It can be deduced from Equations (20) to (25) that these two parameters have predominant influence on the final size distribution. Solutions are obtained for the simple linear variations of the gas temperature and pressure indicated on the figures. These approximately describe the variations through a typical channel-diffuser combination of 20 m in length.

In all three sets of computations, it was considered that 20% of the total slag carryover is in droplet form initially with the mean radius of 2 mm. The initial droplet size is assumed to be distributed according to the Nukiyama-Tanasawa equation (see Williams, 1965):

$$n(0,r) = 130.2\,\frac{N_0}{\bar{r}}\left(\frac{r}{\bar{r}}\right)^4 \exp(5r/\bar{r}) \tag{30}$$

The first set of computations, Figures 2 to 4, was carried out for the initial temperature of 2650°K and ash carryover of approximately 10%. Figure 2 shows the variations with respect to $x$ of the supersaturation ratio and nucleation rate computed by Equations (23) to (25). In the channel ($x \leqq 10$ m) where the supersaturation ratio is below 1, the predominant process is the evaporation of the small size droplets. This results in the disappearance of the small size end, $r < 0.7 \times 10^{-2}$ $\mu$m, of the initial spectrum.

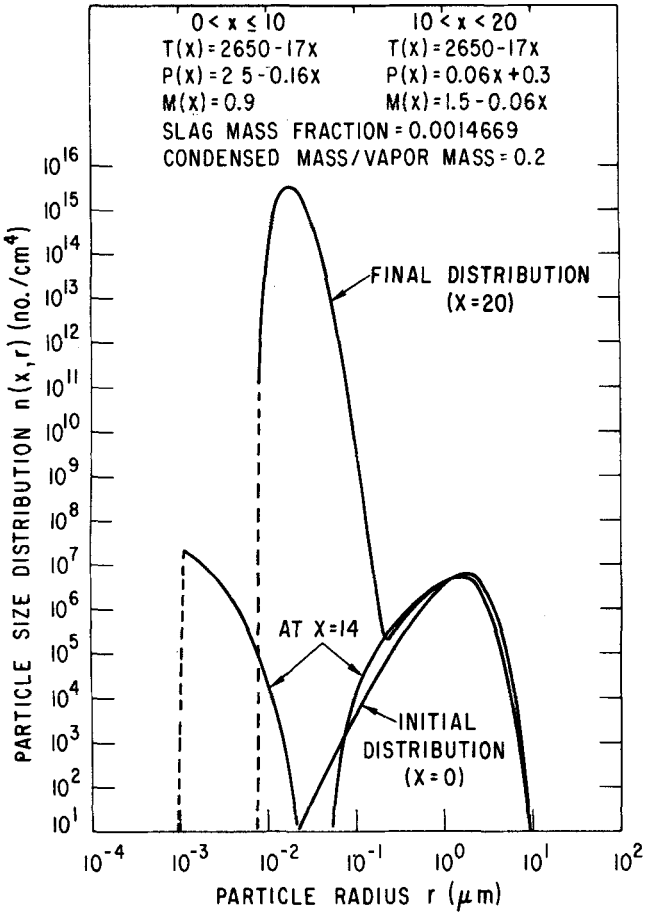


Figure 3. Evolution of size distribution for approximately 10% ash carryover.

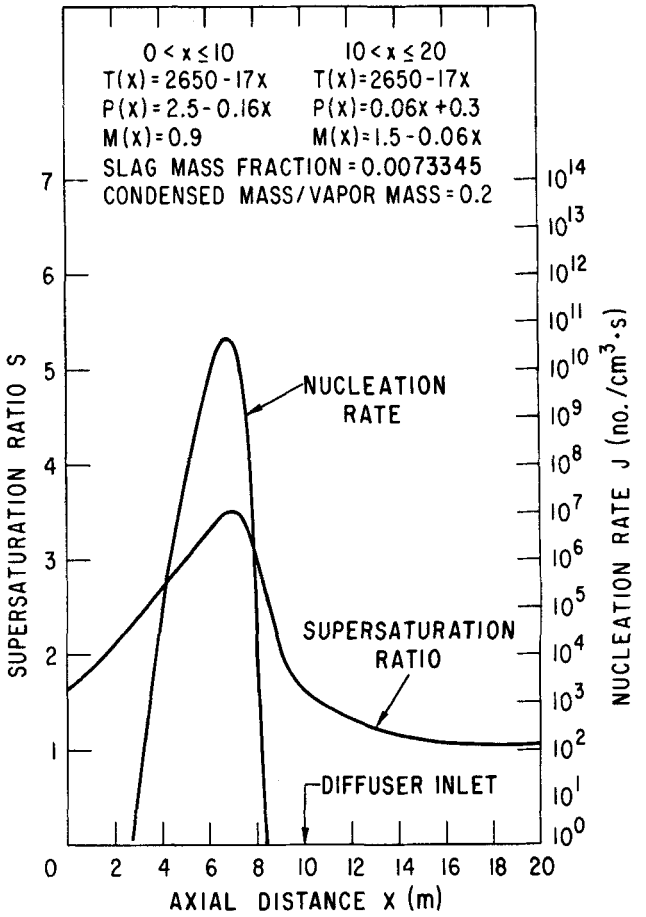


Figure 5. Supersaturation ratio and nucleation rate through channel and diffuser for approximately 50% ash carryover.

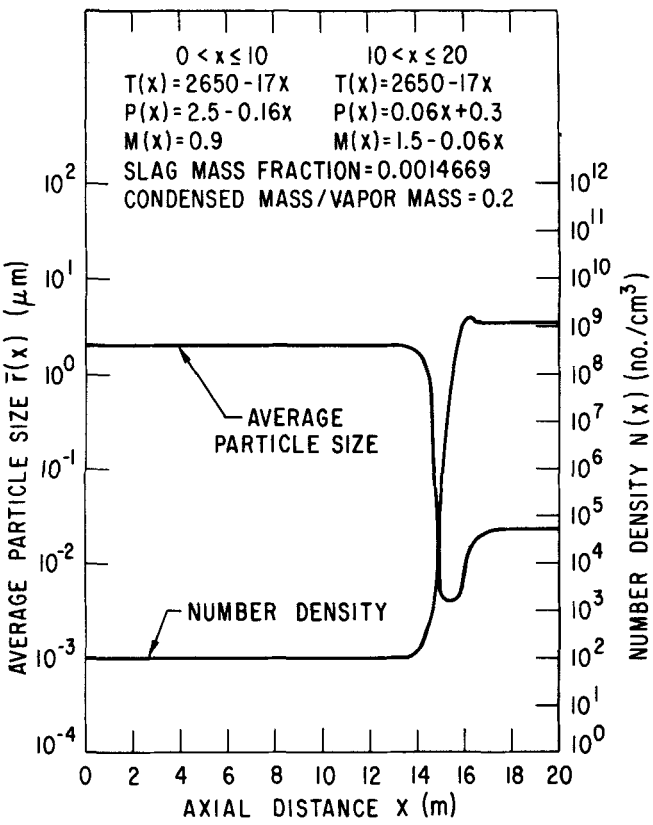


Figure 4. Average droplet radius and total number density for approximately 10% ash carryover.

The supersaturation ratio $S$ increases as the small droplets evaporate in the channel. With the steadily decreasing temperature in the diffuser, $S$ increases at a rapid pace there, and, finally, the nucleation commences rather precipitously.

The size distribution at an early stage of nucleation ($x = 14$ m) is shown on Figure 3. The new arrivals by nucleation comprise the extremely small size end ($r \lesssim 3 \times 10^{-2}$ $\mu$m) of the size spectrum. The size range of $3 \times 10^{-2} \lesssim r \lesssim 8 \times 10^{-2}$ $\mu$m is missing from the spectrum because these particles have either evaporated or have grown into the larger size region by condensation in the diffuser, and at the same time the nucleation which takes place in the smaller size region has not affected the range. The nucleated droplets and the remnant portion of the initial droplet distribution comprise a clearly bimodal size distribution.

The maximum rate of nucleation occurs at $x \approx 16$ m as seen in Figure 2. Figure 4 shows that the total droplet number density rapidly increases, and, at the same time, the mean radius decreases through the nucleation zone.

The total number density and the average droplet radius are evaluated as the first and second moments, respectively, of the size distribution function $n(s, r)\,dr$ as

$$N_0(s) = \int_{r_0}^{\infty} n(s, r)dr \tag{31}$$

$$\bar{r}(x) = \frac{1}{N_0}\int_{r_0}^{\infty} r\, n(s, r)dr \tag{32}$$

The nucleation terminates as precipitously as it began as the nucleation depletes the slag vapor and reduces $S$ to near 1. For the remainder of the diffuser, the small radius region of the spectrum moves into the larger radius region as the droplet growth continues, while nucleation of the small size droplets is

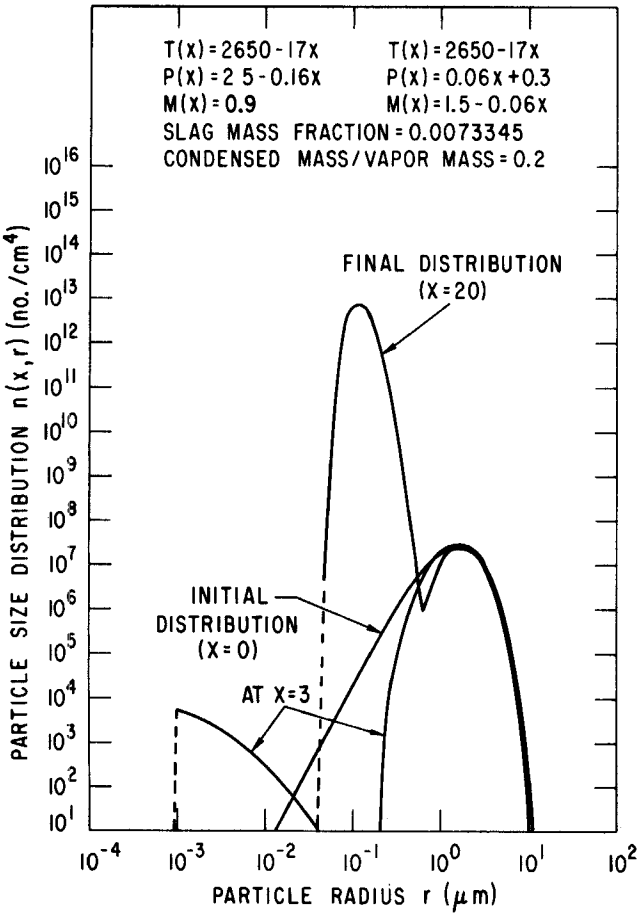


Figure 6. Evolution of size distribution for approximately 50% ash carryover.

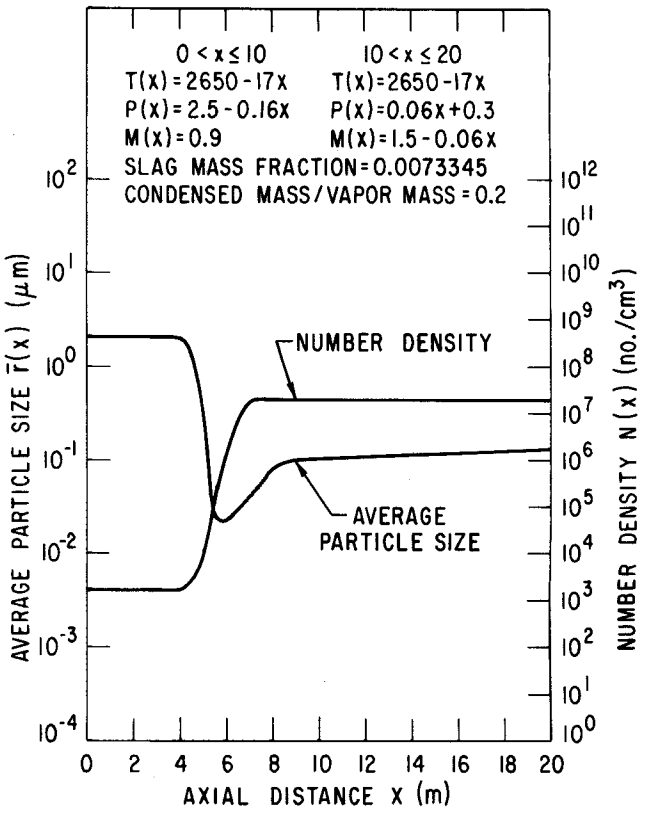


Figure 7. Average droplet radius and total number density for approximately 50% ash carryover.

terminated. The final size distribution as seen in Figure 3 is still distinctively bimodal. This peculiar bimodal distribution is caused largely by the strong size dependence of the growth rate. With the smaller size droplets growing at rates greater than the larger size, an accumulation of the droplet population takes place in a certain relatively narrow size range. The range in which such accumulation takes place for the case of Figure 3 is in the neighborhood of $2 \times 10^{-2}$ $\mu$m, and this range comprises one branch of the bimodal distribution. The other branch consists of the large radius portion ($r > 0.3$ $\mu$m) of the initial distribution which has changed little through the channel and diffuser.

It can be shown from the solution that initially 80% of the mass was associated with the sizes between 1 and 2 $\mu$m. At the end of the diffuser, however, 80% of the slag mass is associated with the droplets of size less than about 0.1 $\mu$m radius.

In closing discussion of the first set of computations, it is noted that the major evolution of the size spectrum took place through the nucleation and subsequent growth of that portion of the slag initially carried into the channel as vapor, and, also, through the evaporation and reappearance of the initial small size droplets into the more numerous and even smaller size droplets.

The second set of computations, Figures 5 to 7, shows the results of an increased S caused by a higher ash carryover. A 50% ash carryover is considered vis-a-vis 10% of the first set. The supersaturation ratio and nucleation rate are shown on Figure 5. The supersaturation ratio is greater than 1 in the channel, and, therefore, no evaporation takes place there. On the contrary, the droplets grow at a steady pace throughout the channel and most portions of the diffuser. S increases in the channel as the temperature is reduced, and the nucleation commences precipitously but rather prematurely in the channel where $x \approx 3$ m. Even though the initial S was much higher for the second set than the first, the S is substantially lower than that for the first case in the nucleation zone. In the first set, a steady accumula-

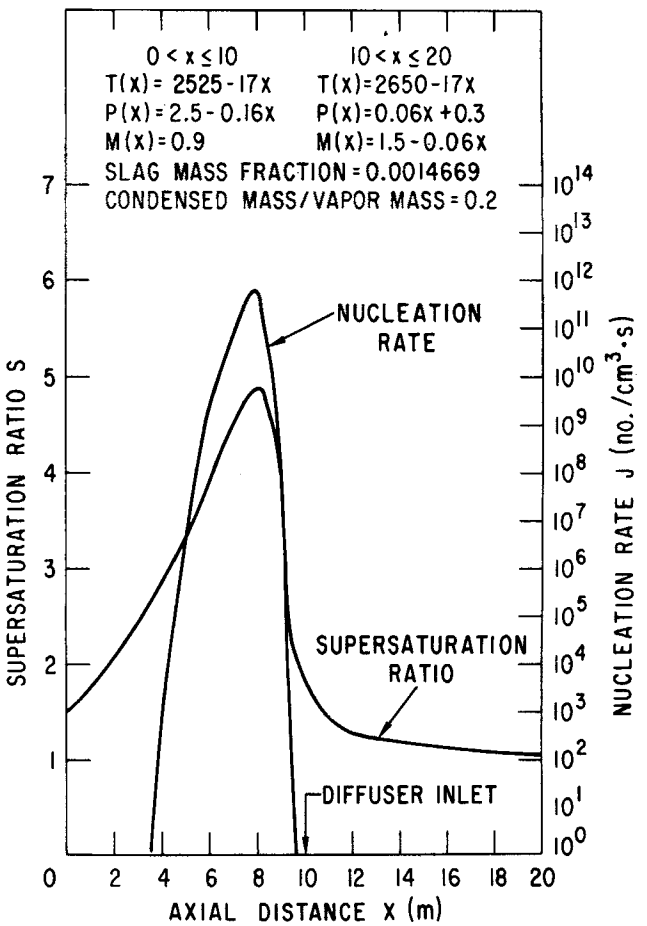


Figure 8. Supersaturation ratio and nucleation rate through channel and diffuser for approximately 10% ash carryover.

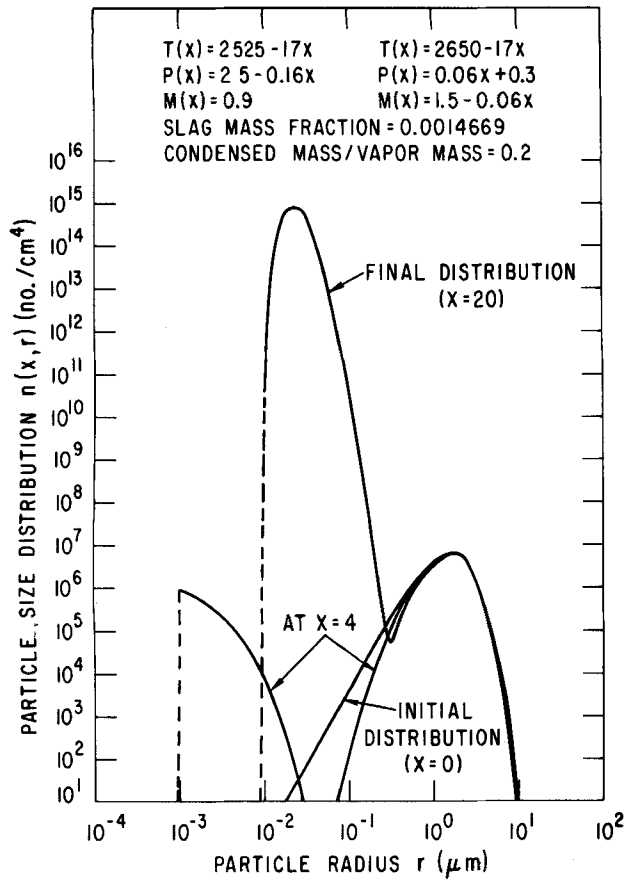


**Figure 9. Evolution of size distribution for approximately 10% ash carryover.**

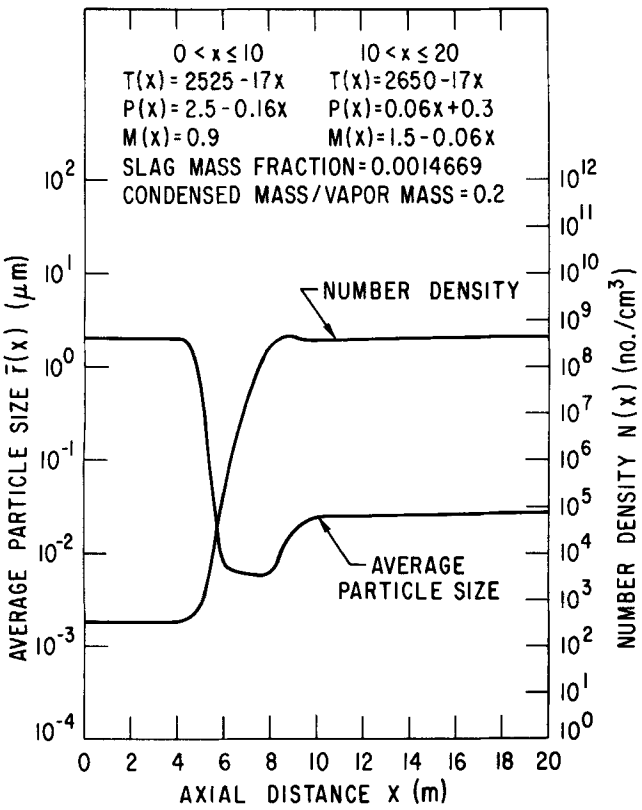


**Figure 10. Average droplet radius and total number density for approximately 10% ash carryover.**

tion of the vapor took place through the channel from evaporation of the small droplets. Therefore, when the nucleation was finally triggered in the diffuser, the supersaturation ratio had reached a very high value. This means that the number of the droplets nucleated in the second set is lower than that in the first set.

In an early stage of nucleation, $x = 3$ m, the size distribution is distinctively bimodal for the same reasons as in the early stage of the set one except that the size range of $5 \times 10^{-2} \lesssim r \lesssim 3 \times 10^{-1}$ $\mu$m is missing from the spectrum because they have grown into the larger size regime through condensation. Because of the high vapor pressure, droplets of this size are rapidly depleted by growth alone, whereas evaporation played a major role in depleting a range of the droplet sizes in set one. Figure 6 shows that the bimodel character of the size distribution persists through the nucleation zone and the diffuser. A comparison of Figures 3 and 6 shows that the size spectrum is generally squeezed toward the larger size region when the slag carryover is raised.

As is seen in Figure 7, the reduced nucleation rate and the increased growth rate of the droplets result in a much reduced number density and a greater mean radius at the end of the diffuser as compared with set one.

In the third set of computations, Figures 8 to 10, the initial supersaturation ratio is the same as that used for the set two. However, this increase of S from set one is obtained by reducing the initial gas temperature rather than by increasing the ash carryover.

As is seen in Figure 8, nucleation takes place approximately at the same position as where it took place in the set two. The peak $S$, however, is higher than that for set two because of the lower gas temperature. The nucleation rate, therefore, is correspondingly higher. The general mode of evolution of the size distribution through the channel and diffuser (see Figures 9 and 10) is the same as those found in the previous sets. The final number density and mean radius are seen in Figure 10 to be of the order of those found in the first set (Figure 4), and are substantially different from the second set (Figure 7). This means that the final total number density and mean radius are strongly influenced by the amount of ash carryover and only moderately by the initial supersaturation ratio.

## ACKNOWLEDGMENT

Work on this paper was performed under the auspices of the U.S. Department of Energy.

## NOTATION

$D_v$ = molecular diffusivity of vapor, m²/s
$G_n^*$ = Gibbs free energy of $n$-mer, J
$I$ = number of particles striking a surface per unit of time, no/s
$J$ = homogeneous nucleation rate, no/s, m³
$k$ = Boltzmann constant = $1.3804 \times 10^9$, J/°K
$K$ = thermal conductivity of gas, J/m · s · K
$Kn$ = Knudsen number, $\lambda/r$
$L$ = heat of vaporization, J/Kg of vapor
$M$ = Mach number
$m$ = mass of a molecule, kg
$N$, $No$ = total droplet number density, no/m³
$n(r, t)$ = droplet number distribution, $N(t) = \int_0^\infty n(r, t)dr$
$n$ = number density of molecules with subscripts, no/m³
$P$ = pressure, N/m²; of gas mixture in stream without subscript
$\dot{r}$ = rate of particle growth, m/s
$r$ = particle radius, m
$r_p$ = scaling constant
$r^*$ = critical radius of droplet, m
$R$ = gas constant, J/kg · °K
$S$ = supersaturation ratio = $P_v/P_{sat}$
$T$ = gas temperature, °K; in stream without subscript
$t$ = time variable, s

$x$ = axial variable, m
$u$ = gas velocity, $M\sqrt{\gamma RT}$
$\hat{v}$ = volume of a vapor molecule, $m^3$
$v$ = average molecular velocity, m/s
$Z$ = Zeldovich factor

**Greek Letters**

$\beta$ = $P_v\, 4\pi(r^*)^2/\sqrt{2\pi R_v T}$
$\delta(r - r^*)$ = Dirac delta function
$\gamma$ = ratio of specific heats, 1.16
$\sigma$ = surface tension of liquid slag, 0.32 N/m
$\lambda$ = mean free path for vapor in stream, m
$\xi$ = radial distance from the center of a droplet, m.
$\rho$ = mass density, $kg/m^3$
$\phi$ = energy function = $2\alpha m_c/\rho_l r$
$\zeta$ = transformed nondimensional variable for $r$ coordinate defined by Equation (28).

**Subscripts**

$b$ = evaluated at nonphysical boundary $b$ in Figure 1
$c$ = condensable species (= vapor)
$g$ = noncondensable gas in stream
$l$ = liquid slag
$s$ = evaluated at the droplet surface
sat = evaluated at saturation
$v$ = vapor in stream
$+$ = toward drop surface from boundary $b$
$-$ = toward the surface $b$ from $s$ in Figure 1

## LITERATURE CITED


Anders, R. P., "Homogeneous Nucleation in a Vapor," in *Nucleation*, A. C. Zettlemayer, ed., p. 69, Marcel Dekker, New York (1969).

Chung, P. M., and R. S. Smith, "An Analysis of a High-Temperature Coal Combustor According to a One-Dimensional Flow Model," ANL/MHD-77-2, Argonne National Laboratory, Argonne, IL. (1977).

Dunning, W. J., *Nucleation*, A. C. Zettlemayer, ed., chapt. 1, Marcel Dekker, New York (1969).

Feder, J., K. C. Russell, J. Lothe and M. Pound, "Homogeneous Nucleation and Growth of Droplets in Vapours," *Adv. in Phys.*, **15**, 111 (1966).

Heywood, H. B., and G. J. Womack, *Open Cycle Power Generation*, Pergamon Press, Oxford, England (1969).

Katz, J. L., and B. J. Ostermier, "Diffusion Cloud-Chamber Investigation of Homogeneous Nucleation," *J. Chem. Phys.*, **47**, 478 (1967).

Kogan, M. N., *Rarified Gas Dynamics*, Translation edited by L. Trilling, Plenum Press, New York (1974).

Lothe, J., and G. M. Pound, "Concentration of Clusters in Nucleation and the Classical Phase Integral," *J. Chem. Phys.*, **48**, 1849 (1968).

Martinez-Sanchez, M., C. E. Kolb and J. L. Kerrebrock, "Potential Effects of Coal Slag Condensation on Plasma Conductivity in MHD Generators," paper presented at the 16th Symposium on Engineering Aspects of MHD, University of Pittsburgh, Aerodyne Research, Inc., ARI-RP-107 (1977).

Reiss, H., and J. L. Katz, "Resolution of the Translation-Rotation Paradox in the Theory of Irreversible Condensation," *J. Chem. Phys.*, **46**, 2496 (1967).

———., and E. R. Cohen, "Translation-Rotation Paradox in the Theory of Nucleation," *ibid.*, **48**, 553 (1968).

Richtmyer, R. D., and K. W. Morton, *Difference Methods for Initial Value Problems*, Interscience, New York (1967).

Sedunov, Y. S., *Physics of Drop Formation in the Atmosphere*, Wiley, New York (1974).

Ubhayaker, K. K., D. B. Stickler, R. E. Gannon and C. W. Von Ronsenberg, Jr., "Devolatilization of Pulverized Coal During Rapid Heating," 16th Symposium Engineering Aspects of MHD, Pittsburgh, Pa. (1976).

Way, S., *Combustion Technology*, H. B. Palmer, and J. M. Bier, ed., Academic Press, New York (1974).

Wegner, P. P., H. A. Clumpner and B. J. C. Wu, "Homogeneous Nucleation and Growth of Ethanol Drops in Supersonic Flow," *Phys. Fluid*, **15**, 1869 (1972).

William, F. A., *Combustion Theory*, Addison-Wesley, Reading, Mass. (1965).



*Manuscript received September 19, 1978; revision received October 15 and accepted October 24, 1979.*


# Mass Transfer in Periodically Cycled Plate Columns Containing Multiple Sieve Plates


**A five plate distillation column, 100 mm in diameter, has been used to study both fluid mixing and the mass transfer separations of mixtures of methylcyclohexane and *n*-heptane under periodically cycled conditions. Both the fluid mixing and mass transfer could be successfully analyzed using the (2S) model to describe the liquid movement in the column. Previously reported results by McWhirter and Lloyd could not be reproduced. Only moderate improvements in separating ability can be obtained with sieve plates and packed sieve plate columns operated in the cycled mode.**



**D. W. GOSS**
**and**
**I. A. FURZER**

**Department of Chemical Engineering**
**University of Sydney, 2006, Australia**


## SCOPE

**Periodic cycling is a method of improving the performance of plate columns by operating with an on-off control of the vapor and liquid flow rates. During the vapor on period, liquid is retained on the plate as downcomerless sieve plates are used in the column. During the vapor off period, liquid drains from a plate to the plates below. The mass transfer theory covering these two periods indicates that the cycled column should operate with separations equivalent to a conventional column containing twice the number of plates. Some experimental results in the early 1960's showed these high levels of performance in multiple sieve plate columns. Other results failed to meet the theoretical improvements in performance. Recently, a good agreement between theory and experiment was obtained on a single sieve plate column. The reason for the mixed literature results is due to a simplistic modeling of the liquid movement down the column during the vapor off period. More elaborate models based on liquid bypassing a plate have been experimentally measured on a number of cycled columns. With multiple sieve plate columns, the fluid mixing during the liquid drain period dominates the mass transfer separation. The following experiments are an attempt to bring together the experimental measurements on fluid mixing and mass transfer separations obtained in a multiple sieve plate column. The method should unify the numerous experimental results reported in the literature on periodic cycling of plate columns.**


D. W. Goss is with ICI Australia.